A Data-Driven Model to Predict Constitutive and Failure Behavior of Elastomers Considering the Strain Rate, Temperature, and Filler Ratio

Aref Ghaderi
Department of Civil Engineering,
Michigan State University,
East Lansing, MI 48823
e-mail: ghaderi1@msu.edu

Roozbeh Dargazany[1]
Department of Civil Engineering,
Michigan State University,
East Lansing, MI 48824
e-mail: roozbeh@msu.edu

This new machine-learned (ML) constitutive model for elastomers has been developed to capture the dependence of elastomer behavior on loading conditions such as strain rate and temperature, as well as compound morphology factors such as filler percentage and crosslink density. It is based on our recent new generation of machine-learning algorithms known as conditional neural networks (CondNNs) Ghaderi et al. (2020, "A Physics-Informed Assembly of Feed-Forward Neural Network Engines to Predict Inelasticity in Cross-Linked Polymers," Polymers, 12(11), p. 2628), and uses data-infused knowledge-driven machine-learned surrogate functions to describe the quasi-static response of polymer batches in cross-linked elastomers. The model reduces the 3D stress-strain mapping space into a 1D space, and this order reduction significantly reduces the training cost by minimizing the search space. It is capable of considering the effects of loading conditions such as strain rate, temperature, and filler percentage in different deformation states, as well as enjoying a high training speed and accuracy even in complicated loading scenarios. It can be used for advanced implementations in finite element programs due to its computing efficiency, simplicity, correctness, and interpretability. It is applicable to a variety of soft materials, including soft robotics, soft digital materials (DMs), hydrogels, and adhesives. This model has a distinct advantage over existing phenomenological models as it can capture strain rate and temperature dependency in a much more comprehensive way. [DOI: 10.1115/1.4056705]

Keywords: constitutive modeling, artificial neural network, soft materials, Mullins effect, strain rate, computational mechanics, constitutive modeling of materials, mechanical properties of materials, micromechanics

1 Introduction

Cross-linked polymer products are widely used in various applications ranging from medical gloves to shock absorbers due to their lightweight, low-cost, durability, and resilience of elastomers. So far, significant efforts have been made toward developing accurate and affordable models to describe the nonlinear mechanical behavior of cross-linked polymers or to predict their failure points [1–3]. Finite strain theory and fracture mechanics are widely used in most developed models. However, very few models can predict elastomers' nonlinear constitutive and failure behavior at the same time [4–6].

Constitutive Behavior. The constitutive models of elastomeric components, which are typically stated by explicit functions within the context of continuum mechanics, are generally very important for their design and optimization [7,8]. Numerous studies have been conducted on and applications made to conventional continuum mechanics-based constitutive models for the numerical analysis of engineering structures. These models, however, are only as precise as their underlying assumptions [9].

The Mullins effect, which is known to make it difficult to construct a hyperelastic strain function that accurately reflects the stress-strain response in filled rubber, has a few key characteristics. These include a notable decrease in stiffness when it is unloaded after the first cycle, an even greater reduction in stiffness when the initial strain is higher, minimal softening when the initial strain is not exceeded during subsequent cycles, and a minor but persistent set that stays consistent through all following cycles [10–12].

The permanent set normally rises after unloading from a higher maximum strain; however, occasionally, it might recover following a significant period of rest. The Mullins effect has been extensively studied in the literature in an effort to link it to a variety of factors, including quasi-irreversible structural changes in filler configuration, chain- slippage, and network damage.

Classification of Cross-Linked Polymers Response. Figure 1 depicts two loading cycles in the uniaxial tensile test to demonstrate this phenomenon. A virgin particle-filled rubber specimen is loaded to extend $\lambda^{(1)}$ on Path 1 and then unloaded to the stress-free state on Path 2. When the external stress is fully removed, the unloading curve intersects the positive λ axis at the stretch $\lambda_{re}^{(1)}$, which is the residual extension remaining in the specimen. The stress-stretch curve leads to Path 3 when the specimen is reloaded to a stretch $\lambda^{(2)}$ greater than $\lambda^{(1)}$. The specimen is then unloaded along Path 4, with a wider residual stretch $\lambda_{re}^{(2)}$ remaining. At the same stretch level, the stress along Path 2 (Path 4) is significantly less than that along Path 1 (Path 3) due to the stress-softening effect. The permanent set is the remaining stretch after full unloading, which may gradually decrease over time. In fact, according to experimental findings [12], the reloading curve after a loading

[1]Corresponding author.

Contributed by the Applied Mechanics Division of ASME for publication in the Journal of Applied Mechanics. Manuscript received November 16, 2022; final manuscript received January 13, 2023; published online February 8, 2023. Assoc. Editor: Pradeep Sharma.

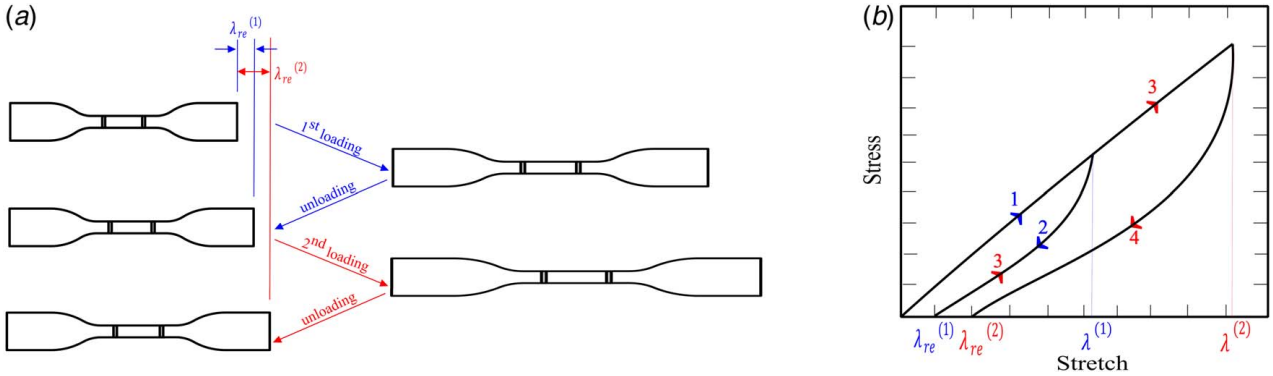

Fig. 1 The Mullins effect schematic with a permanent set: (*a*) two uniaxial tensile cycles deformation based on ASTM D412-C [13] and (*b*) the related stress-stretch curves

period is lower than the virgin material's first loading curve but higher than the unloading curve. The hysteresis phenomenon is the difference between the unloading and reloading directions. The strain rate effects are responsible for this phenomenon [10,11].

Cross-linked polymers have strong nonlinear elasticity associated with inelastic effects in their overall behavior. Because of the underlying polymer microstructure inside the polymer matrix, amorphous polymers display rate-dependent finite elastic-plastic behavior. The realignment of kinks, rearrangement of convolutions, reorientation, and uncoiling of molecular chains as the load is accommodated results in this behavior. Temperature fluctuation, on the other hand, can have an impact on the mechanical characteristics of these materials. They may be exposed to the outdoors or have internal heating as a result of energy dissipation. The majority of theoretical and experimental research on this topic has been done at room temperature [14]. However, these materials' mechanical characteristics should be explored at temperatures other than room temperature. The interaction between the filler and the polymer matrix is also affected by temperature changes. As a result, filled polymers display more complicated nonlinear behavior that is temperature-dependent. As a result, developing a temperature-dependent and filler-dependent, strain rate constitutive model that predicts the inelastic behavior of cross-linked polymers in various states of deformation for a wide range of strain, strain rate, temperature, and filler concentration to be applicable for various types of operations is extremely important and challenging.

Constitutive Approaches to Model Strain Rate of Soft Materials. Phenomenological models, which are based on a collection of material properties, do not take into account the microphysics of materials [5,12]. Micromechanical analysis, on the other hand, is based on the statistical mechanics of polymer structure and uses physical meaning in its analysis. Micromechanical models that include functions and material factors linked to microstructure take into account microstructural data; however, their practical applicability is restricted owing to their high computing costs and lengthy training procedure.

With the increase of the computational capacity, data-driven approaches can address the limits of the analytical models derived based on continuum mechanics. Recently, increasing attention has been given to developing data-driven approaches that are directly derived based on material data. Tang et al. [15,16] proposed a mechanistic-based, data-driven approach for numerical analysis, and they demonstrated that this mechanistic-based approach could exploit the deep physical insights obtained from well-established finite strain theory and experimental evidence. At the same time, this approach can circumvent issues in establishing explicit functions to characterize material behaviors, which is necessary for classical CDM theory [17].

In this contribution, a physics-informed data-driven strain rate model was developed to predict the constitutive and failure behavior of the cross-linked polymers that integrates conditional artificial neural networks (CNNs) into continuum reconfiguration. The data-driven constitutive model developed in this study can consider the synergistic effect of strain rate, temperature, polymer type, and filler ratio. A practical two-step method is proposed in the data training stage, enabling highly effective training using only a small amount of experimental data. To validate the approach, the proposed method was applied to investigate the mechanical behaviors of natural rubber (NR) and styrene-butadiene rubber (SBR) under various loading conditions. Our proposed network architecture has several advantages compared to other researches. First, it is able to integrate strain rate, temperature, and filler percentage together with physics to accurately predict the behavior of elastomers, allowing for more accurate predictions. Second, it uses a deep learning approach that enables the model to learn the complex interactions between the different parameters, allowing it to make more accurate predictions than traditional approaches. Finally, by incorporating physics into the model, it provides a more comprehensive understanding of how the elastomer behaves, allowing for more accurate predictions.

The paper is organized as follows. Section 2 presents a description of knowledge infusion through the hard implementation of governing laws such as continuum mechanics and polymer physics. Section 3, the setup of our engine and its dependence on external loads and compound properties, e.g., different strain rates, filler percentages, and temperatures, is described. Section 4 presents a demonstration of the developed data-driven model, in which the model is used to predict the strain rate-dependent and temperature-dependent mechanical response of the cross-linked polymer, and it also includes a discussion of the results. Conclusions based on the research findings are provided in Sec. 5.

2 Directional Physics-Informed Model

The rise of machine-learned (ML) models has gotten a lot of press in recent decades. For modeling the mechanical behavior of rubbery media, the first generation of "black-box" ML models was presented as another sort of phenomenological model [18–20]. Note that the high degrees-of-freedom of these approaches makes them obsolete due to the high demand for data for training.

Stress-strain tensors in solid mechanics are only partially visible in lower dimensions. As a result, acquiring data to feed the black-box ML model is quite challenging. As a result, physics-informed neural networks (PINNs) represent the best of the two previously described methodologies in the next generation of ML models. To put it another way, PINN seeks to overcome the limits of both phenomenological and micromechanical models by extracting microstructural behavior from macroscopic experimental data [21,22].

Model-free distance minimization approaches eliminate the usage of constitutive models by explicitly selecting stress-strain couples with the shortest distance to experimental data while maintaining compatibility and equilibrium restrictions [23,24].

Dimension-reduction methods attempt to construct a constitutive manifold from experimental data to explain a close approximation of the strain energy in various states of deformation. [25,26]. To capture the high-dimensional and non-smooth behavior of the material, ML models are employed to derive surrogate functions as reduced-order models of multi-scale approaches. The approach has been proven to be a promising strategy in multi-scale research [27,28]. In this contribution, a physics-informed data-driven nonlinear rate-dependent constitutive model is proposed based on our recent work on implementing knowledge into neural network (NN) models, which captures not only compounding ratios but also temperature and strain rate effects.

2.1 Constitutive Behavior: Mechanical and Environmental Damages. The experimental results show that an elastomeric sample exposed to parallel evolution behaves in a mode that may be characterized as hyperelastic with accumulated mechanical and environmental damages. Accordingly, two phenomena, (i) chemical evolution and (ii) mechanical evolution, brought on the damaging buildup in the elastomers.

The major objective of this part is to define suitable matrix energy taking the evolution precursor $\mathcal{E}$ into account. We define $0 < \varepsilon < 1$ as a general non-kinematic scalar parameter, taking into account effective factors for evolution accumulation, to describe the overall state of evolution in relation to the evolution brought on by mechanical and environmental forces.

2.2 Mechanical Damage: Cooperative Multi-Agents System. Through the hard implementation of the physical laws into the neural network, we already discussed how the mechanical damage in constitutive behavior of polymer matrix could be represented by cooperative multi-agent system $\mathcal{A}_j^i, i \in \{1,n\}, j \in \{1,m\}$, based on our last study [29]. The model can explain different features in the material behavior with $n*m$ different learning agents. The objective is to minimize the collective error between the predicted system performance and the experimental data. Each agent is trained to provide a specific material behavior that minimizes the total error. To bring all of the agents back into a centralized system, model fusion is employed. Our model represents each agent by a simple deep-learned neural network constrained by the hard implementation of physical laws into a neural network.

Constitutive behavior of the virgin material is modeled based on our recent paper [29] using a set of collaborative shallow neural network agents.

In our recent paper, we suggested a framework to use ideas from continuum mechanics, statistical physics, and polymer science to create super-constrained reduced-order machine learning algorithms, which could partially solve the present challenges. We have simplified the 3D stress-strain tensor mapping problem into a small set of super-constrained 1D mapping problems via sequential order reduction. Then, we added a collection of numerous replicated neural network learning agents (L-agents) to categorize those mapping issues into a select few groups, each of which was described by a different sort of agent. Accordingly, the polymer matrix continuum has been represented by a microsphere constructed by polymer chains that are uniformly and equally dispersed in all spatial directions. Micro-sphere concept is valid for materials that are initially isotropic and incompressible. The volumetric strain energy of the microsphere was then expressed by integrating the energy of chains in all directions as $[\boldsymbol{d}_i]_{i=1\ldots N_d}$. Assuming the 3D polymer matrix to be a homogeneous super-assembly of various 1D polymer bundles dispersed in all spatial directions, the energy of the sphere, Ψ_m, may be easily calculated by integrating the energies of all the components, as

$$\Psi_m = \frac{1}{4\pi}\int_S \Psi_m^d dS^d \tag{1}$$

Using this approach, the behavior of the polymer matrix can be modeled by having the behavior of basic 1D components. To calculate the energy of all 1D components, a surface integration may be carried out numerically across N_d integration directions $[\boldsymbol{d}_i]_{i=1\ldots N_d}$ with different weight factors $[w_i]_{i=1\ldots n}$. Such integration can be performed by discretizing the sphere into finite sections. Therefore, it is possible to express the strain energy of the polymer matrix Ψ_m in terms of its constituents as

$$\Psi(\boldsymbol{F}) = \frac{1}{4\pi}\int_S \psi^d dS^d \cong \sum_{i=1}^{N_d} w_i \psi^{d_i}, \text{ where } \psi^{d_i} = \mathcal{B}^{d_i} \tag{2}$$

where $\boldsymbol{F}$ stands for macro-scale deformation gradient, ψ^{d_i} is the element's energy in direction d_i and is represented by a group of L-agents $\mathcal{B}^{d_i}$ that, using the microsphere idea, represents the cooperative addition of many L-agents $\mathcal{B}^{d_i} = \sum_{j=1}^{N_s} \mathcal{A}_j^{(i)} = \sum_{j=1}^{N_s} \mathcal{N}_j^{(i)}(\boldsymbol{x}_e, \Theta_e)$. We assume that, in the virgin state, $\mathcal{B}^{d_i} = \mathcal{B}^{d_j}$, all multi-agents are identical in order to meet initial isotropy. It is crucial to reformat the energy of a single polymer chain with respect to $\lambda^d = \sqrt{\boldsymbol{d}^T \boldsymbol{F}^T \boldsymbol{F} \boldsymbol{d}}$ as follows because chains in different orientations are subject to multiple micro-stretches. As a result, we may directly extract the matrix's energy in terms of sub-elements and L-agents.

$$\Psi_m = \frac{1}{4\pi}\int_S \Psi_m^d dS^d \cong \sum_{i=1}^{N_d}\sum_{j=1}^{N_s} w_i \psi_j^{d_i} := \sum_{i=1}^{N_d}\sum_{j=1}^{N_s} w_i \mathcal{A}_j^i \tag{3}$$

If each sub-element is characterized by an L-agent, a simplified feed-forward neural network will represent the super-simplified scalar-to-scalar mapping behavior of the sub-element. The first Piola–Kirchhoff stress tensor P may be calculated using Eqs. (1) and (3) to summarize the enforced restrictions.

$$\mathbf{P} = \frac{\partial \Psi_m}{\partial \boldsymbol{F}} - p\boldsymbol{F}^{-T} := \sum_{i=1}^{N_d}\sum_{j=1}^{N_s} w_i \frac{\partial \mathcal{A}_j^i}{\partial \boldsymbol{F}} - p\boldsymbol{F}^{-T} \tag{4}$$

where p is the Lagrange multiplier used to assure the material's incompressibility. P may therefore be written as

$$\begin{aligned}\mathbf{P} &= \frac{\partial \Psi_M(\boldsymbol{F})}{\partial \boldsymbol{F}} - p\boldsymbol{F}^{-T}, \ \frac{\partial \Psi_M(\boldsymbol{F})}{\partial \boldsymbol{F}} \\ &= \sum_{i=1}^{k} w_i \frac{\partial \mathcal{B}^{d_i}}{\partial \lambda^{d_i}} \frac{1}{2\lambda^{d_i}} \frac{\partial d_i \bar{\mathbf{C}} d_i}{\partial \bar{\boldsymbol{F}}} : \frac{\partial \bar{\boldsymbol{F}}}{\partial \boldsymbol{F}}, \text{ while } \psi^{d_i} = \mathcal{B}^{d_i}\end{aligned} \tag{5}$$

where $\mathbf{C}$ is the right Cauchy–Green tensor, $\bar{\boldsymbol{F}} = \boldsymbol{J}^{-1/3}\boldsymbol{F}$, and $\bar{\mathbf{C}} = \boldsymbol{J}^{-2/3}\mathbf{C}$. Additionally, by applying the following identities, Eq. (5) might be made even simpler as follow:

$$\frac{\partial d\bar{\mathbf{C}} d}{\partial \bar{\boldsymbol{F}}} : \frac{\partial \bar{\boldsymbol{F}}}{\partial \boldsymbol{F}} = 2\bar{\boldsymbol{F}}(\boldsymbol{d}\otimes\boldsymbol{d}) : \boldsymbol{J}^{-\frac{1}{3}}\mathbb{I} = 2\boldsymbol{J}^{-\frac{1}{3}}\bar{\boldsymbol{F}}(\boldsymbol{d}\otimes\boldsymbol{d}) \tag{6}$$

Normalization, conditions of growth, isotropy, objectivity, and poly-convexity are already satisfied in the proposed equation in our recent paper [29].

2.3 Environmental Damage: Multiplicative Decomposition of Strain Energy. The effects of loading scenarios, material morphology, and environmental conditions on rubber behavior are generally considered inelastic. From a modeling aspect, inelastic effects can be described through a collection of chemical and physical events within the matrix. However, establishing the relationship between the chemical/physical evolution of the matrix and the changes in macro-performance remains a significant challenge in physics-based modeling. On the contrary, the data-driven models do not need to establish this relationship explicitly and thus can directly describe the strain energy of the matrix through multiplicative decomposition to describe the effects of physical $\mathcal{E}_p$ and chemical $\mathcal{E}_p$ evolutions on the strain energy of a sub-element as

$$\psi_j^{d_i} = \mathcal{E}_p \mathcal{E}_c \psi_{0;j}^{d_i} \tag{7}$$

where $\psi_j^{d_i}$, and $\psi_{0;j}^{d_i}$ denote the updated and reference energy of a sub-element in the network j and direction d_i damaged portion.

Almost all external inelastic effects can be described using multiplicative chemical and physical evolution parameters, ranging from aging and degradation to hyperelasticity and creep.

- **Reversible physical changes**. $\mathcal{E}_p$ mainly involves deformation-induced changes in the material and often heals over time. Thus, $\mathcal{E}_p$ gradually tends toward one with time. It is mainly induced by the breakage of ionic bonds, the recoverable hyperelastic motion of free chains, and the slippage of elastically active cross-linked chains. In filled elastomers, physical evolution can be further induced by the sliding between fillers and filler-rubber matrix, the breakage and reformation of agglomerates, and the deformation of elastic aggregates. These mechanisms also induce physical stress relaxation, cyclic hysteresis, and often healing. Within the context of this paper, deformation-induced mechanical damages are mainly described by maximum microstretch in history $\lambda^d_{\max}$ and classified as physical changes. One can approximate $\mathcal{E}_p$ as a deep neural network (DNN) with following parameters:

$$\mathcal{E}_p = \mathcal{N}_p(\boldsymbol{x}_p, \Theta_p^{(i)}),\ \{\lambda^d \in \boldsymbol{x}_p, \lambda^d, \lambda^d_{\max}\} \tag{8}$$

- **Maximum microstretch in history** $\lambda^d_{\max}$. In the course of deformation, polymer chains begin to slide on or debond from the aggregates. This debonding starts with the shortest chain and gradually involves longer and longer chains. Under unloading, the debonded chains do not reattach back to the aggregate's active sites, and thus the maximal microstretch previously reached in the loading history

$$\lambda^d_{\max} = \max_{\tau\in(-\infty,t]} \lambda^d(\tau) \tag{9}$$

  is crucial for the description of the polymer-filler debonding.
- **Irreversible chemical changes**. $\mathcal{E}_c$ mainly involves the **unrecoverable** inelastic events, and thus $\mathcal{E}_c$ remains constant or go toward zero over time. Unrecoverable molecular changes in the cross-linked network are often manifested by the breakage of covalent bonds and the formation of a "plastic-like" behavior upon complete unloading, i.e., permanent set. The chemical evolution can lead to competing mechanisms such as scission or formation of chemical bonds and crosslink formation, which are also influenced by rubber compounds such as the ratio of antioxidants, fillers, etc. Within the context of this paper, the effects of the aging condition, compounding ratios, and external temperatures are mainly described by chemical evolution. One can approximate $\mathcal{E}_c$ as a DNN with following parameters:

$$\mathcal{E}_c = \mathcal{N}_c(\boldsymbol{x}_c, \Theta_c^{(i)}),\ \{n, T\} \in \boldsymbol{x}_c \tag{10}$$

In general, we outline two key requirements that $\mathcal{E}_p$ and $\mathcal{E}_c$ must meet

(1) $\mathcal{E}_p$ should always move toward one with time,
(2) depending on the situation, $\mathcal{E}_c$ will stay the same or go toward zero over time.

3 Strain Energy of the Damage Matrix

Given the multiple multiplicative elements involved in deriving the strain energy of the damaged matrix, we proposed using a conditional neural network (CondNN) to represent the energy of each L-agent. The reason for the importance of this is having a model to predict superficial damage in non-aged material and also predict hardening in virgin but aged material.

3.1 Conditional Neural Network L-Agent. A simple N-layer multilayer feed-forward neural network comprising an input layer, $N-1$ hidden layers, and an output layer. We suppose that the nth hidden layer has N_n neurons. The previous layer's post-activation output $\boldsymbol{x}^{n-1} \in \mathbb{R}^{N_{n-1}}$ is then fed into the nth hidden layer, and the specific affine transformation is of the form

$$\mathcal{H}_n(\boldsymbol{x}^{n-1}) \triangleq \boldsymbol{W}^{(n)}\boldsymbol{x}^{n-1} + \boldsymbol{b}^{(n)} \tag{11}$$

where the network weight $\boldsymbol{W}^{(n)} \in \mathbb{R}^{N_n \times N_{n-1}}$ and the bias term $\boldsymbol{b}^{(n)} \in \mathbb{R}^{N_n}$ to be learned are both initialized using unique procedures like Xavier or He initialization [30,31].

The nonlinear activation function $\sigma(.)$ is applied component-by-component to the current layer's affine output $\mathcal{H}_n$. Furthermore, for some regression issues, this nonlinear activation is not employed in the output layer. As a result, the neural network may be denoted as

$$\mathcal{N}(\boldsymbol{x}; \boldsymbol{\Theta}) = (\mathcal{H}_N \circ \sigma \circ \mathcal{H}_{N-1} \circ \cdots \circ \sigma \circ \mathcal{H}_1)(\boldsymbol{x}) \tag{12}$$

where $\circ$ denotes the composition operator, $\Theta = \{\boldsymbol{W}^{(n)}, \boldsymbol{b}^{(n)}\}_{n=1}^{N} \in \mathcal{P}$ denotes the learnable parameters to be optimized later in the network, and $\mathcal{P}$ denotes the parameter space, and $\mathcal{N}$ and $x^0 = x$ denote the network's output and input, respectively.

CondNNs are a continuum of machine-learned models which are hybrids of two extreme machine learning algorithms, computationally efficient trees, and super-accurate neural networks (see Refs. [32,33]). CondNNs lie in between the two extremes, and we can tune the hyperparameters to generate CondNNs with different efficiency/accuracy trade-offs. By using the routing feature from the decision tree, CondNNs can use conditional routing to confine computation to only a small region of the network rather than involving all nodes. Such capability makes CondNNs particularly relevant for complex problems where the outputs are not only dependent on past events, such as deformation-induced matrix damages, but also on external data, which can be loading conditions or compound properties (Fig. 2).

Routed behavior, in which data are transmitted to one or more children depending on a learned routing function, is a characteristic of decision trees. In other words, CondNNs are decision trees with the difference that instead of nodes, shallow NNs are being used (see Fig. 3). Note that we can use routing conditions to derive physical or chemical evolution parameters or a combination thereof. Also, such architecture can be scaled to include other external effects such as aging, creep, swelling, or plasticity (Fig. 4).

Conditional neural networks are advantageous in comparison to simple neural networks because they can be used to provide chances for more efficient and effective learning. These networks allow for the learning process to be tailored to specific conditions, meaning that the network can better adjust to the data it is given and can better predict future outcomes. This allows for more accurate and detailed predictions, as the network can adjust itself to the conditions that are being presented to it. Additionally, conditional neural networks allow for more efficient and effective learning as they can better identify patterns and make better predictions, leading to faster and more accurate results.

– *Engine setup with multiple CondNNs.* The hyperparameters summary and inputs determine the design of the neural network: (i) the number of hidden layers, n_l (network depth), (ii) the number of neurons per hidden layer, n_n (network width), and (iii) the activation function. So, we can write

$$\mathcal{E}_p = \mathcal{N}_p(\boldsymbol{x}_p, \Theta_p^{(i)}),\ \mathcal{E}_c = \mathcal{N}_c(\boldsymbol{x}_c, \Theta_c^{(i)}),\ \psi^{d_i}_{0;j} = \mathcal{N}_e(\boldsymbol{x}_e, \Theta_e^{(i)}) \tag{13}$$

Next, we define the loss function L mean squared error for a total of n_{tot} data points as

$$\mathcal{L}(\boldsymbol{x}, \Theta) = \frac{1}{2}\sum_{n=1}^{n_{\text{tot}}}\left[\boldsymbol{g}_1\left(\sum_{i=1}^{N_d}\sum_{j=1}^{N_s} w_i \frac{\partial\left(\mathcal{E}_p\mathcal{E}_c\psi^{d_i}_{0;j}\right)}{\partial \mathbf{F}} - p\mathbf{F}^{-T}\right)\boldsymbol{g}_1 - P_n^{11}\right]^2 \tag{14}$$

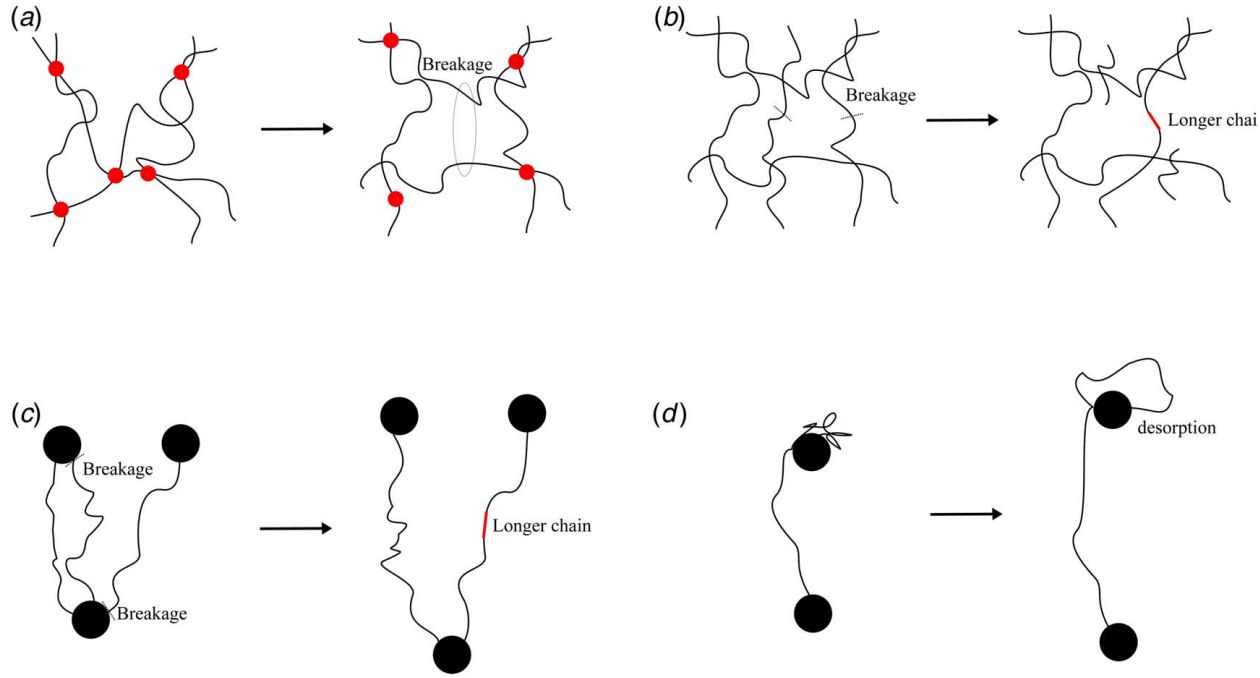

Fig. 2 (*a*) The breakage of chain crosslinks, (*b*) chain scission, (c) the bond rupture of rubber-particle linkages, and (*d*) desorption of chains from particle surfaces

where $P_n^{11} := \boldsymbol{g}_1 \mathbf{P} g_1$ is the first component of the experimental macro-scale stress tensor $\mathbf{P}_n$ in loading direction g_1 for point n.

4 Experimental Validation

For benchmarking, the proposed engine has been trained and validated in four different loading scenarios

(1) Digital materials (DMs) that promote relaxation.
(2) Modeling strain rate effects on uniaxial tension and compression.
(3) Modeling individual and combination of the temperature and filler ratio effects on constitutive behavior.
(4) Modeling coupled effects of the temperature and strain rate on constitutive behavior.

To evaluate engine's prediction at different stages of deformation, the predictions were benchmarked against experimental data in all scenarios.

4.1 Engine Architecture. We employed an identical engine to mimic both loading scenarios, and the engine is made by $N_d = 21$ teams, each with $N_s = 2$ L-agents [34]. It is worth noting that the number of teams and associated L-agents were determined based on the accuracy/efficacy trade-off. We evaluated one input layer, one hidden layer with four neurons, and three activation functions soft plus $\psi(\cdot) = \ln(1 + e)$, sinusoid $\psi(\cdot) = \sin(\cdot)$, and hyperbolic tangent $\psi(\cdot) = \tan \mathrm{h}(\cdot)$ for the CondNNs structure of L-agents. We are employing a shallow network to guarantee the convergence of finite element method analysis.

To capture the deformation of the rubbers with complete memory, the internal parameters of L-agents were developed using $\lambda_{j-\max}$ parameters. The first and second deformation invariants were provided to each team in order to allow them to anticipate possible deformation states [35]. The requirement was met by feeding input sets to the first and second L-agents in the following order:

$$\boldsymbol{x}_p^{(i)} = [\lambda^{d_i}, \dot{\lambda}^{d_i}, \lambda_{\max}^{d_i}], \boldsymbol{x}_c^{(i)} = [T], \boldsymbol{x}_e^{(i)} = [n, \dot{\lambda}^{d_i}, \lambda_{\max}^{d_i}] \tag{15}$$

while

$$\lambda^{d_i} = \sqrt{d_i \mathbf{C} d_i}, \mathbf{C} = \boldsymbol{F}^T \boldsymbol{F} \tag{16}$$

where λ^{d_i} is connected to I_1, as the first invariants of $\mathbf{C}$.

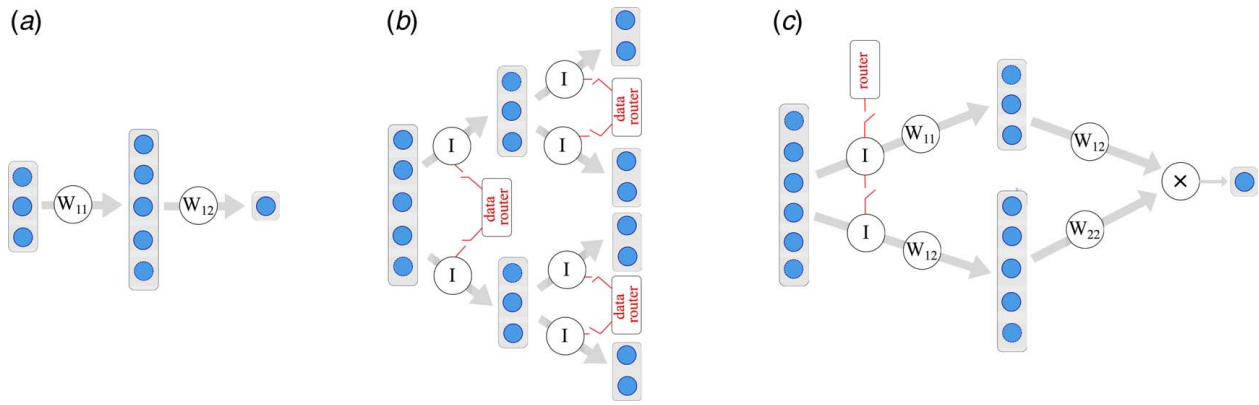

Fig. 3 Schematic figures for (*a*) a compact graphical notation for neural networks, (*b*) a representing decision trees, and (*c*) a generic conditional network

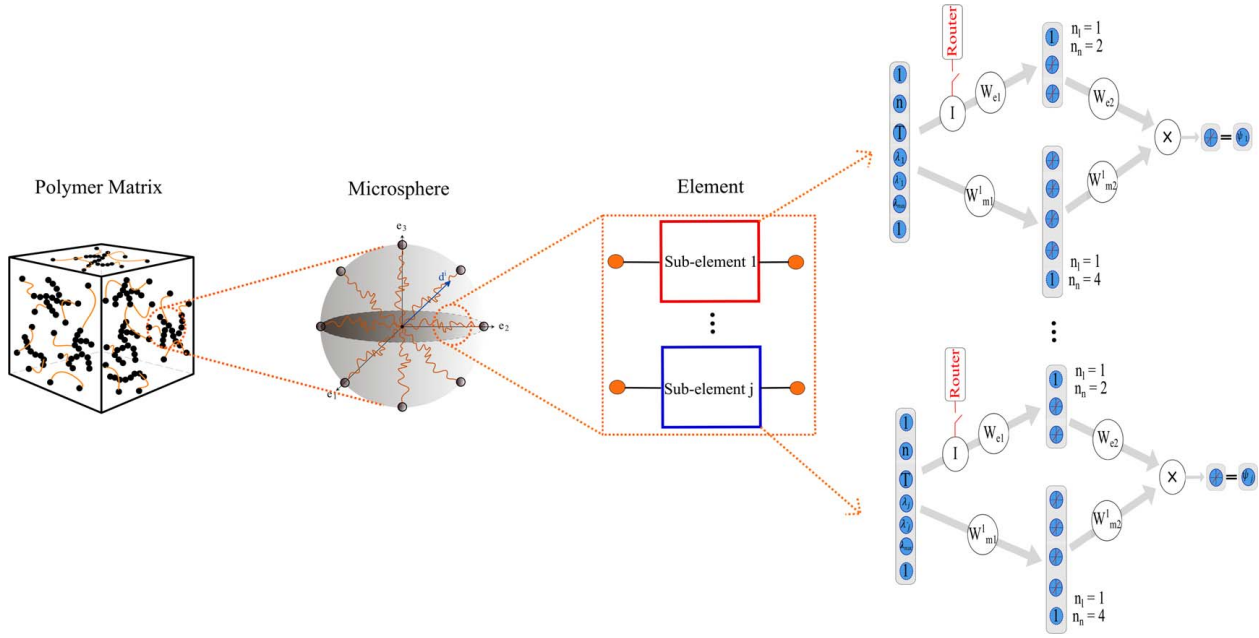

Fig. 4 Illustration of the suggested model, which includes order reduction and model fusion. It demonstrates how we propose a knowledge-based platform using ideas from continuum mechanics, polymer sciences, physics, and machine learning.

In conclusion, the rubber matrix was represented as a cooperative game with 21 teams of two agents through $\mathcal{A}_j^i, i \in \{1,21\}, j \in \{1,2\}$. The ultimate cost function of the engine after agent fusion is given as

$$\mathcal{L}(\boldsymbol{x}, \Theta) = \frac{1}{2}\sum_{n=1}^{n_{\text{tot}}} \left[\boldsymbol{g}_1 \left(\sum_{i=1}^{21} \sum_{j=1}^{2} w_i \frac{\partial \mathcal{A}_j^i}{\partial \lambda_j^{d_i}} \frac{\partial \lambda_j^{d_i}}{\partial \mathbf{F}} - p\boldsymbol{F}^{-T} \right) \boldsymbol{g}_1 - P_n^{11} \right]^2 \tag{17}$$

assuming $\lambda_{\max} \leqslant 0$, and weights related to λ, and $\dot{\lambda} \geqslant 0$ to satisfy thermodynamic consistency and poly-convexity, respectively.

Training Procedure. For history-dependent materials, internal parameters should be used to feed the L-agent parameters that specifically represent the material's damage. For defining various materials, however, different sorts of damage parameters would be necessary. For example, internal parameters should convey information from one iteration to the next for materials having recent memory, such viscoelastic materials. As an example, the maximum stretch and temperature in rubber material may be utilized as a damage antecedent to display the history of damage in each direction. In contrast, for materials with complete memory, such as elastomers, the internal parameters can be established independently of the solution iterations. Therefore, each L-agent in every direction has damage parameters. Because we cannot train agents in situations in which they are not involved or have a little part to play, we must train using biaxial dataset.

As a result, confidence in agent training is closely correlated with the quality of the training data and the contribution of the agents in certain circumstances. By characterizing the quality of data in relation to the input required by each agent, we may assess the confidence interval within which an agent may be taught with high confidence with regard to the given data. Low-quality data might result in inaccurate conclusions that seem to be fully solid, while too little data can obscure important details and give us a false sense of confidence.

The purpose of training with several deformation states is to demonstrate the performance of the model using various datasets.

The model can forecast various states of deformation depending on the ranges that the model has calibrated based on uniaxial tensile data up to stretch χ. The prediction ranges should fall inside the area where the agent has been trained in order to guarantee good model prediction (for more information, please see Ref. [29]).

These training/prediction domains may be estimated for various training and prediction scenarios with various deformation states, as shown in Table 1. It should be noted that while the model may

Table 1 Prediction domain for train until stretch χ

Training prediction	Uniaxial tensile	Biaxial tensile	Pure shear	Uniaxial compression	Plane strain compression
Uniaxial tensile	χ	χ	χ	$\frac{1}{\sqrt{\chi}}$	$\frac{1}{\chi}$
Biaxial tensile	$\sqrt[4]{\chi}$	χ	$\sqrt[4]{\chi}$	$\frac{1}{\sqrt{\chi}}$	$\frac{1}{\chi}$
Pure shear	χ	χ	χ	$\frac{1}{\sqrt{\chi}}$	$\frac{1}{\chi}$
Uniaxial compression	$\frac{1}{\sqrt{\chi}}$	$\frac{1}{\chi^2}$	$\frac{1}{\chi}$	χ	χ
Plane strain compression	$\frac{1}{\sqrt{\chi}}$	$\frac{1}{\chi^2}$	$\frac{1}{\chi}$	χ	χ

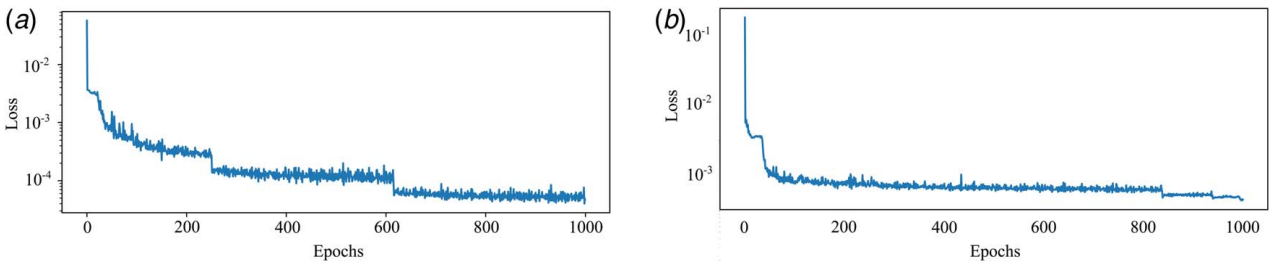

Fig. 5 Convergency in the training of proposed NN model with experimental dataset: (*a*) carbon black-filled rubber and (*b*) polyurea behavior at high strain rates

extrapolate and make predictions outside the confidence range, they are not always reliable.

The number of data points that we are using for training is equal to the number of points for experimental data, which has been shown in the figures. Also, Fig. 5 shows the error to the number of iterations after training related to tensile tests on carbon black-filled rubber and polyurea behavior at high strain rates.

Grid search is a powerful tool for hyperparameter selection and can help to identify the optimal set of hyperparameters for a given model. Based on that, we tuned the model's hyperparameter such that a range of hyperparameters and their respective values are identified, and the performance of each set of hyperparameters is evaluated. The set of hyperparameters that yields the best performance is then selected as the optimal set of hyperparameters that should be used. Also, the model training time is less than a few minutes due to the simplicity of the model. However, the time can be reduced by using more powerful hardware, such as GPUs or multiple CPUs, in order to speed up the training process.

Results for Elastomers. We assess the performance of the suggested model in this part using experimental data from multiple elastomers in various rate ranges. First, we look at uniaxial deformations since evaluating the effectiveness of suggested models in simple deformations, which are easier to test, is a standard method (actually, most available data in the literature are for uniaxial tension or uniaxial compression). The following set of data was used for benchmarking (see Table 2).

- **High damper rubber (HDR) compression experiment**. Our engine was validated against monotonic HDR compression experiments at low to moderate strain rates [36]. To eliminate the Mullins effect, each virgin specimen was exposed to five pre-loading cycles before the actual test, as described in Ref. [36]. Our engine predictions and the experimental data are in strong agreement, as shown in Fig. 6(*a*). HDR's behavior did not show a significant shift at rates higher than 0.88/*s*, according to Ref. [36]. Note that dot lines have been used for training and the solid lines show the performance of the model in prediction after the training.
- **Tensile tests on carbon black-filled rubber** [37]. After removing the Mullins effect, the experiments were carried out on five different specimens using monotonic strain-controlled tension. The tests were performed at low to moderate strain rates, and the data are recorded as nominal stress versus stretch. When compared to the experimental data, the performance is illustrated in Fig. 6(*b*). Note that dot lines have been used for training and the solid lines show the performance of the model in prediction after the training.
- **Polyurea behavior at high strain rates** using a drop weight tensile testing device [38]. In view of the high flexibility and economic feasibility of polyurea, the high rate-dependent deformation behavior of polyurea was used for benchmarking. The comparison against experiments is shown in Fig. 6(*c*). Experiments show that at rates exceeding 400/*s*, the material's behavior becomes nearly rate-independent, which is exactly what the model predicts.
- **Uniaxial tensile test at different temperatures**. Seasonal temperature changes can cause significant variations in the mechanical properties of rubber. Therefore, the impact of temperature on the mechanical properties of rubber must be considered. Although the mechanical responses of filled and unfilled rubber have been characterized at room temperature, the effects of temperature on the mechanical response of rubber materials in a certain deformation range have rarely been studied [39]. Four types of rubber materials filled with different contents of carbon black were used in this study [39]. The rubber matrix was natural rubber, and the filled carbon black was N234. The proposed model has been benchmarked against these results to show the performance of the model in predicting the effects of temperature on the mechanical response of rubber materials (see Fig. 7).
- **Uniaxial tensile tests on styrene-butadiene rubber with different filler ratios**. The data of four styrene-butadiene rubbers filled with 30, 40, 50, or 60 phr carbon black N347 and constructed of the identical gum composition were used to validate our engine's predictive capabilities [40]. Each material softens to some extent when loaded to maximum strain, and this is reflected in a gentler reaction when unloaded. The comparison against experiments is shown in Fig. 8. Note that dot lines have been used for training and the solid lines show the performance of the model in prediction after the training.

Table 2 The summary of the experimental datasets used for benchmark

Material	Loading type	Feature	References
HDR	Compression	Strain rate	[36]
Black filled rubber	Uniaxial	Strain rate	[37]
Polyurea	Uniaxial	High strain rate	[38]
Rubber	Uniaxial	temperature	[39]
SBR	Uniaxial	Filler ratio	[40]
PVA	Uniaxial	Temperature and strain rate	[41]

Results for Polyvinyl Acetate (PVA). We have previously shown that our constitutive model can properly predict uniaxial tension test data for elastomers. Uniaxial tension tests for dual-crosslink PVA [41] at various temperatures, and strain rates may also be accurately predicted, as shown below. We forecast the stress-stretch curve for uniaxial constant stretch rate tension tests using weights gained during model training and compare these predictions to test outcomes. Model predictions are compared to three temperature and two loading rate tests in Fig. 9. There is a high agreement between model predictions and experimental evidence. Fitting is shown by dashed lines, whereas prediction is represented by solid lines.

Results for Digital Materials. In this paragraph, we use the weights derived from very high bonding (VHB) 4910's stress relaxation training to demonstrate the model's relaxation capture ability. The VHB was loaded at a stretch rate of $\dot{\lambda} = 0.1613/s$, as shown in Fig. 10(*b*). This sample is stretched at a set pace, and once it reaches $\lambda = 2, 4, 6$ it is held in that stretch for 900*s* before being loaded

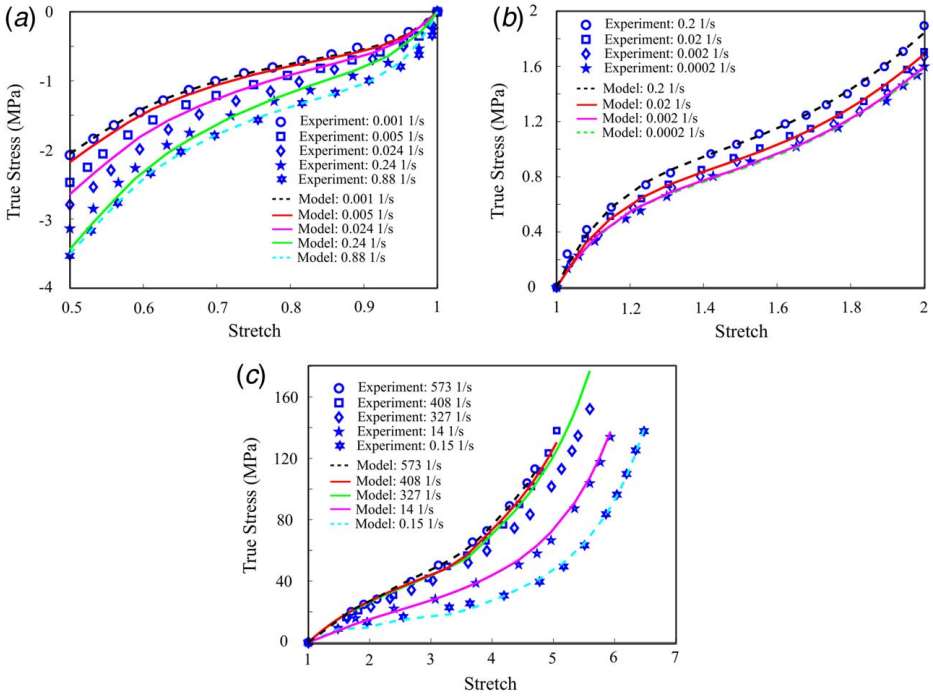

Fig. 6 (*a*) Comparison of the proposed model results with [36] nonlinear's uniaxial compression test data for high damping rubber, (*b*) comparison of the proposed model results with [37] uniaxial extension test data for carbon black filled rubber, and (*c*) comparison of the proposed model results with [38] uniaxial extension test data for polyurea. Fitting is shown by dashed lines, whereas prediction is represented by solid lines.

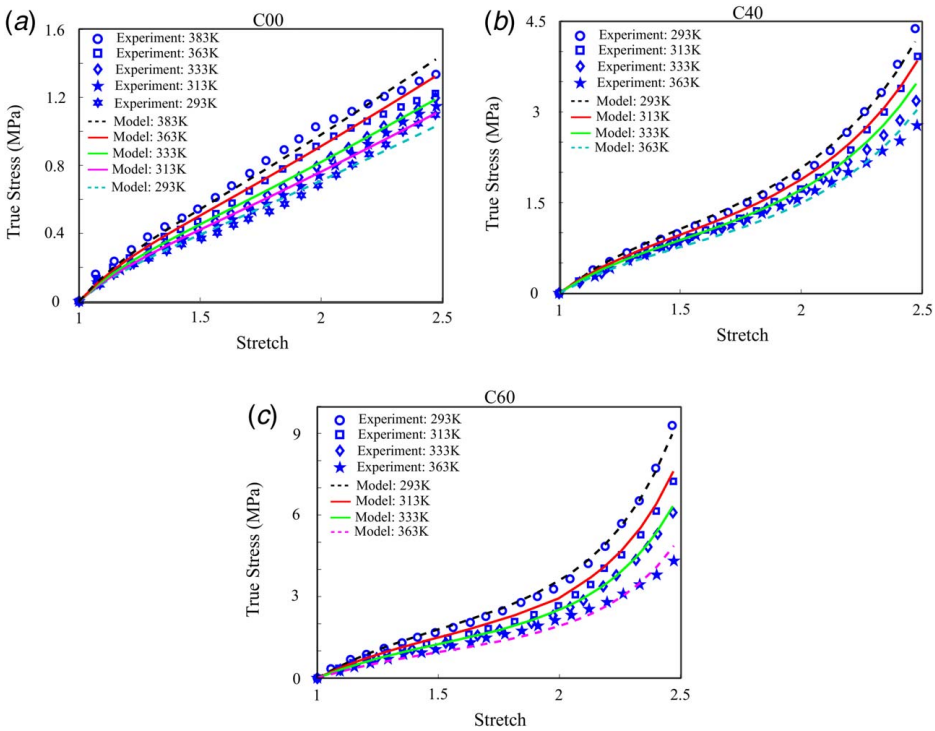

Fig. 7 Based on the suggested model and the uniaxial extension test results provided by Ref. [39], stress-strain curves of three types of carbon black-filled vulcanized rubber compounds (*a*) C00, (*b*) C40, and (*c*) C60 at different temperatures. Fitting is shown by dashed lines, whereas prediction is represented by solid lines.

again. When it hits the $\lambda_{max} = 7$ maximum stretch, it is emptied at the same pace. Please read this article [43] for more information. The experiment's outcome is depicted in Fig. 10(*a*). Our strain rate model can well capture the relaxation behavior of VHB in loading, relaxing, and unloading operations, as illustrated in Fig. 10. Note that due to the lack of using convolution integral in our model, it is not able to predict behavior that has a different situation from the training dataset.

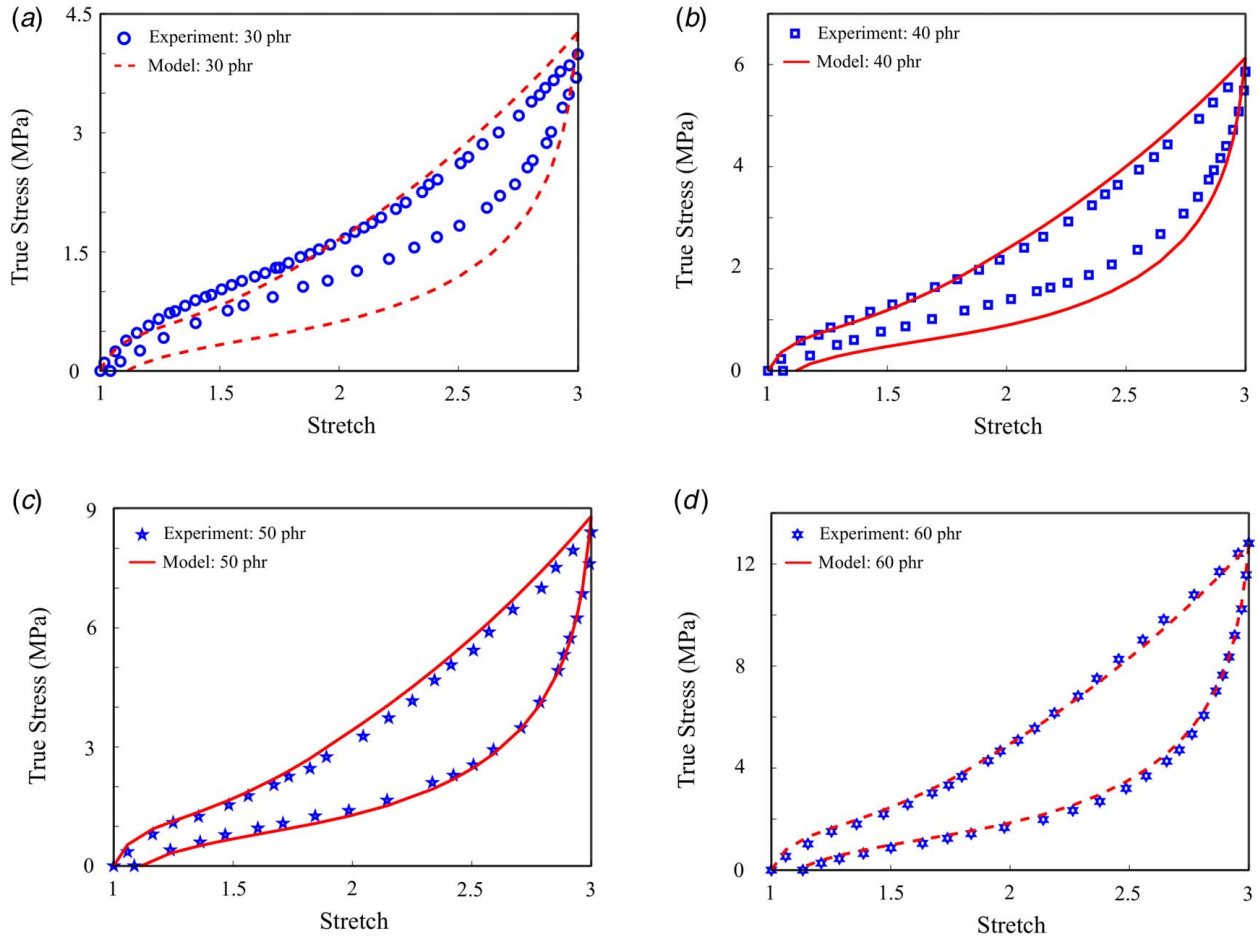

Fig. 8 The suggested model was used to compare the outcomes of four rubbers manufactured of the same SBR gum and filled with either (*a*) 30, (*b*) 40, (*c*) 50, or (*d*) 60 phr of N347 carbon black when they were subjected to cyclic uniaxial loading-unloading, as described by Ref. [40]. Fitting is shown by dashed lines, whereas prediction is represented by solid lines.

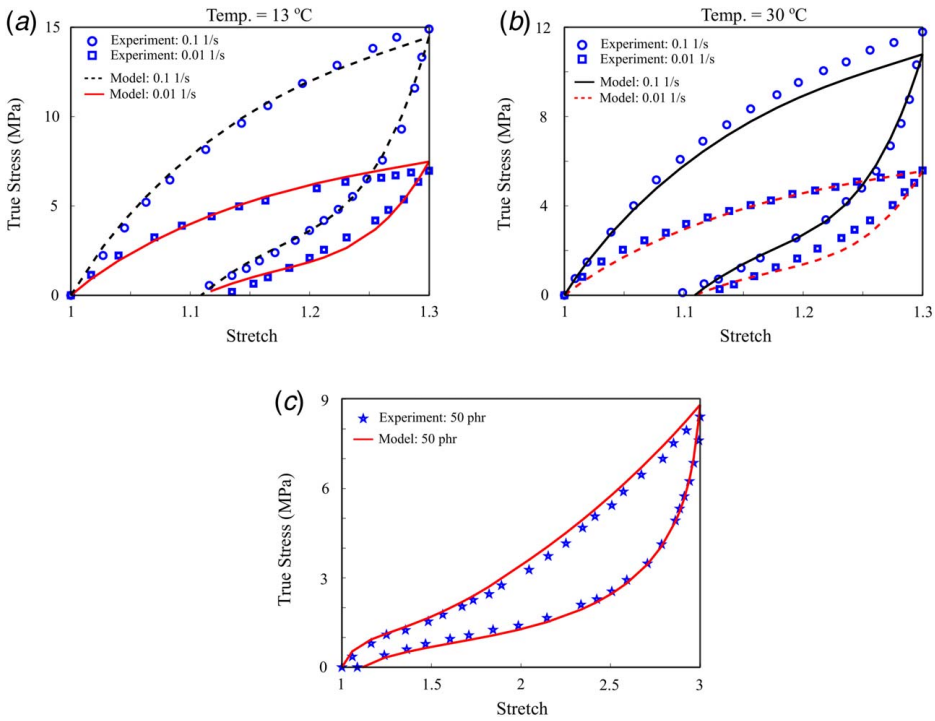

Fig. 9 Reference [42] provided a comparison of model and experimental testing at two distinct stretch rates and temperatures of (*a*) 13 °C, (*b*) 30 °C, and (*c*) 50 °C. Fitting is shown by dashed lines, whereas prediction is represented by solid lines.

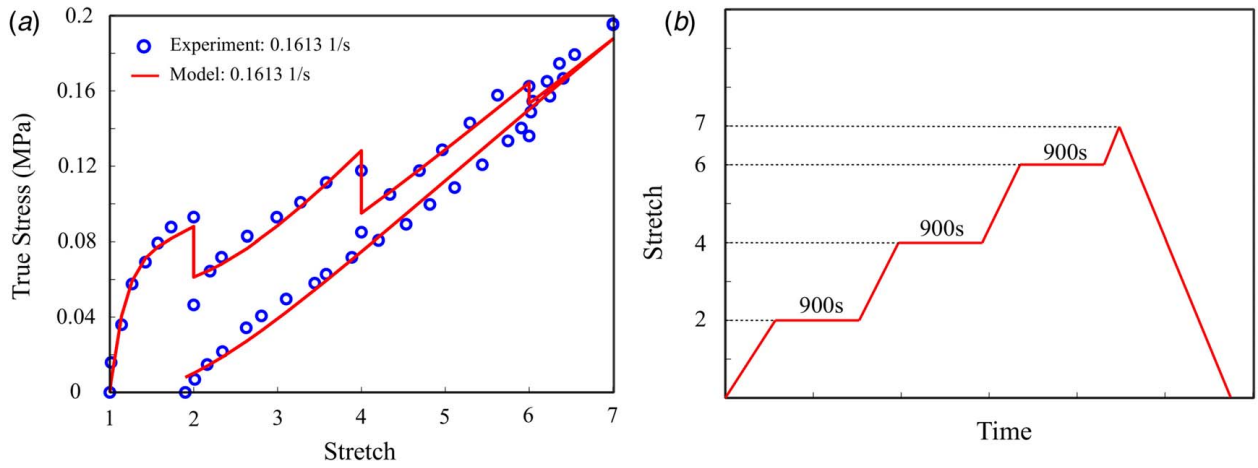

Fig. 10 (*a*) Comparison of the model results and experimental data of stress-stretch relations for VHB 4910 at loading rate $\dot{\lambda}$ = 0.1613/s and (*b*) experimental method of sequential relaxation experiment [43]

5 Summary

The purpose of this study was to expand our most recent model, [29], to include the impacts of strain rate, temperature, and percentage of filler without sacrificing the accuracy of the prior model in order to make the previous model more complete. To anticipate the inelastic hyperelastic behavior of soft materials, a large strain three-dimensional physics-informed data-driven model was developed. Despite significant attempts to predict hyperelasticity and its influence on the mechanical performance of soft materials, there have been few models that can concurrently account for strain rate, temperature, and filler percentage with acceptable computational resources. By order reduction into a 1D mapping issue, we used polymer science, statistical physics, machine learning, and continuum mechanics techniques to simplify 3D stress-strain tensor mapping. The mechanical behavior of VHB 4910, elastomers, and hydrogel was predicted using our model. The results reveal that our model accurately describes the hyperelastic behaviors of soft materials. Based on the findings of the proposed model on various datasets, the following conclusions may be drawn: (1) the suggested model has predicted rubber stress-strain curves at various strain rates that were in good agreement with the experimental data. The developed model may, therefore, properly represent the hyperelastic mechanical behavior of soft materials over a specified deformation range, (2) the devised approach was evaluated for its ability to represent the temperature dependency of elastomer mechanical performance, and (3) the suggested model was used to create a filler-dependent model with specific filler quantity parameters. At various filler quantities, the explicit filler quantity model may adequately explain the hyperelastic mechanical behavior of rubber. Because of its computing speed, simplicity, correctness, and interpretability programs for FE, the model is an excellent choice for advanced implementations. Note that hybrid methods combine data-driven and physics-based approaches to tackle complex problems. While these methods often have the advantage of combining the best of both worlds, they also present certain limitations. Data-driven methods rely on large amounts of training data to approximate a solution. This reliance on data means that these methods are limited by the quality and quantity of the data available. If the data are incomplete or noisy, the resulting solution may be inaccurate. Additionally, data-driven methods do not take into account any physical or theoretical constraints. On the other hand, physics-based methods rely on theoretical models to approximate a solution. These models are often complex and require a great deal of knowledge to implement correctly. Additionally, physical laws are often too restrictive and may not capture all of the complexity of a problem. The limitations of hybrid methods arise from the limitations of both data-driven and physics-based methods. Hybrid methods combine the best of both approaches, but they are still limited by the availability of data and the complexity of the physical models. Hybrid methods are also limited by the time and effort required to develop and implement them. Finally, hybrid methods tend to be more difficult to interpret, as they combine the complexity of both data-driven and physics. Also, the shape and size of the sample in tensile testing have a direct effect on the output of the test. The shape of the sample affects the stress-strain curve, which is the output of the test. The size of the sample affects the maximum load that can be applied before the sample fails. In general, larger specimens have higher ultimate tensile strengths than smaller specimens because they are able to resist larger loads. The shape of the sample also affects the stress-strain curve because different shapes will have different stress-strain curves. For example, a round sample will have a different stress-strain curve than a rectangular sample. However, the model works as long as the stress-strain curves are based on the same standards.

Conflict of Interest

There are no conflicts of interest.

Data Availability Statement

The datasets generated and supporting the findings of this article are obtainable from the corresponding author upon reasonable request.

References

[1] Mao, G., Huang, X., Liu, J., Li, T., Qu, S., and Yang, W., 2015, "Dielectric Elastomer Peristaltic Pump Module With Finite Deformation," Smart Mater. Struct., **24**(7), p. 075026.
[2] Li, T., Zou, Z., Mao, G., Yang, X., Liang, Y., Li, C., Qu, S., Suo, Z., and Yang, W., 2019, "Agile and Resilient Insect-Scale Robot," Soft Robot., **6**(1), pp. 133–141.
[3] Yin, T., Wu, T., Zhong, D., Liu, J., Liu, X., Han, Z., Yu, H., and Qu, S., 2018, "Soft Display Using Photonic Crystals on Dielectric Elastomers," ACS Appl. Mater. Interfaces, **10**(29), pp. 24758–24766.
[4] Dal, H., Zopf, C., and Kaliske, M., 2018, "Micro-Sphere Based Viscoplastic Constitutive Model for Uncured Green Rubber," Int. J. Solids Struct., **132**, pp. 201–217.
[5] Kaliske, M., and Rothert, H., 1997, "Formulation and Implementation of Three-Dimensional Viscoelasticity at Small and Finite Strains," Comput. Mech., **19**(3), pp. 228–239.
[6] Volokh, K., 2010, "On Modeling Failure of Rubber-Like Materials," Mech. Res. Commun., **37**(8), pp. 684–689.
[7] Dal, H., Açıkgöz, K., and Badienia, Y., 2021, "On the Performance of Isotropic Hyperelastic Constitutive Models for Rubber-Like Materials: a State of the Art Review," ASME Appl. Mech. Rev., **73**(2), p. 020802.

[8] Karapiperis, K., Stainier, L., Ortiz, M., and Andrade, J., 2021, "Data-Driven Multiscale Modeling in Mechanics," J. Mech. Phys. Solids, **147**, p. 104239.
[9] Frankel, A., Hamel, C. M., Bolintineanu, D., Long, K., and Kramer, S., 2022, "Machine Learning Constitutive Models of Elastomeric Foams," Comput. Meth. Appl. Mech. Eng., **391**, p. 114492.
[10] Ayoub, G., Zaïri, F., Naït-Abdelaziz, M., Gloaguen, J. M., and Kridli, G., 2014, "A Visco-Hyperelastic Damage Model for Cyclic Stress-Softening, Hysteresis and Permanent Set in Rubber Using the Network Alteration Theory," Int. J. Plast., **54**, pp. 19–33.
[11] Guo, Q., Zäuri, F., and Guo, X., 2018, "A Thermo-Viscoelastic-Damage Constitutive Model for Cyclically Loaded Rubbers. Part II: Experimental Studies and Parameter Identification," Int. J. Plast., **101**, pp. 58–73.
[12] Diani, J., Brieu, M., and Vacherand, J., 2006, "A Damage Directional Constitutive Model for Mullins Effect With Permanent Set and Induced Anisotropy," Eur. J. Mech. A Solids, **25**(3), pp. 483–496.
[13] R. I. Annually, 1995, ASTM Standards.
[14] Rodas, C. O., Zaïri, F., Naït-Abdelaziz, M., and Charrier, P., 2015, "Temperature and Filler Effects on the Relaxed Response of Filled Rubbers: Experimental Observations on a Carbon-Filled SBR and Constitutive Modeling," Int. J. Solids Struct., **58**, pp. 309–321.
[15] Tang, S., Li, Y., Qiu, H., Yang, H., Saha, S., Mojumder, S., Liu, W. K., and Guo, X., 2020, "Map123-EP: A Mechanistic-Based Data-Driven Approach for Numerical Elastoplastic Analysis," Comput. Meth. Appl. Mech. Eng., **364**, p. 112955.
[16] Liu, X., Tian, S., Tao, F., and Yu, W., 2021, "A Review of Artificial Neural Networks in the Constitutive Modeling of Composite Materials," Compos. B. Eng., **224**, p. 109152.
[17] Tang, J., Chen, X., Pei, Y., and Fang, D., 2016, "Pseudoelasticity and Nonideal Mullins Effect of Nanocomposite Hydrogels," ASME J. Appl. Mech., **83**(11), p. 111010.
[18] Shen, Y., Chandrashekhara, K., Breig, W., and Oliver, L., 2004, "Neural Network Based Constitutive Model for Rubber Material," Rubber Chem. Technol., **77**(2), pp. 257–277.
[19] Liang, G., and Chandrashekhara, K., 2008, "Neural Network Based Constitutive Model for Elastomeric Foams," Eng. Struct., **30**(7), pp. 2002–2011.
[20] Song, G., Chandrashekhara, K., Breig, W., Klein, D., and Oliver, L., 2005, "J-Integral Analysis of Cord-Rubber Serpentine Belt Using Neural-Network-Based Material Modelling," Fatigue Fract. Eng. Mater. Struct., **28**(10), pp. 847–860.
[21] Raissi, M., Perdikaris, P., and Karniadakis, G. E., 2019, "Physics-Informed Neural Networks: A Deep Learning Framework for Solving Forward and Inverse Problems Involving Nonlinear Partial Differential Equations," J. Comput. Phys., **378**, pp. 686–707.
[22] Raissi, M., and Karniadakis, G. E., 2018, "Hidden Physics Models: Machine Learning of Nonlinear Partial Differential Equations," J. Comput. Phys., **357**, pp. 125–141.
[23] Kirchdoerfer, T., and Ortiz, M., 2016, "Data-Driven Computational Mechanics," Comput. Methods Appl. Mech. Eng., **304**, pp. 81–101.
[24] Nguyen, L. T. K., and Keip, M.-A., 2018, "A Data-Driven Approach to Nonlinear Elasticity," Comput. Struct., **194**, pp. 97–115.
[25] Amores, V. J., Benítez, J. M., and Montáns, F. J., 2019, "Average-Chain Behavior of Isotropic Incompressible Polymers Obtained From Macroscopic Experimental Data. A Simple Structure-Based WYPiWYG Model in Julia Language," Adv. Eng. Softw., **130**, pp. 41–57.
[26] Ibanez, R., Abisset-Chavanne, E., Aguado, J. V., Gonzalez, D., Cueto, E., and Chinesta, F., 2018, "A Manifold Learning Approach to Data-Driven Computational Elasticity and Inelasticity," Arch. Comput. Meth. Eng., **25**(1), pp. 47–57.
[27] Reimann, D., Nidadavolu, K., ul Hassan, H., Vajraguptaul Hassan, H., Glasmachers, N., Junker, T., and Hartmaier, P., 2019, "Modeling Macroscopic Material Behavior With Machine Learning Algorithms Trained by Micromechanical Simulations," Front. Mater., **6**, pp. 181.
[28] Zopf, C., and Kaliske, M., 2017, "Numerical Characterisation of Uncured Elastomers by a Neural Network Based Approach," Comput. Struct., **182**, pp. 504–525.
[29] Ghaderi, A., Morovati, V., and Dargazany, R., 2020, "A Physics-Informed Assembly of Feed-Forward Neural Network Engines to Predict Inelasticity in Cross-Linked Polymers," Polymers, **12**(11), p. 2628.
[30] Glorot, X., and Bengio, Y., 2010, "Understanding the Difficulty of Training Deep Feedforward Neural Networks," Proceedings of the Thirteenth International Conference on Artificial Intelligence and Statistics, JMLR Workshop and Conference Proceedings, Chia Laguna Resort, Sardinia, Italy, May 13–15.
[31] He, K., Zhang, X., Ren, S., and Sun, J., 2015, "Delving Deep Into Rectifiers: Surpassing Human-Level Performance on Imagenet Classification," Proceedings of the IEEE International Conference on Computer Vision, Santiago, Chile, Dec. 7–13.
[32] Wang, E., Kosson, A., and Mu, T., 2017, Deep Action Conditional Neural Network for Frame Prediction in Atari Games, Technical Report, Stanford University.
[33] Ioannou, Y., Robertson, D., Zikic, D., Kontschieder, P., Shotton, J., Brown, M., and Criminisi, A., 2016, "Decision Forests, Convolutional Networks and the Models In-Between," arXiv preprint.
[34] Ehret, A., Itskov, M., and Schmid, H., 2010, "Numerical Integration on the Sphere and Its Effect on the Material Symmetry of Constitutive Equations—A Comparative Study," Int. J. Numer. Meth Eng., **81**(2), pp. 189–206.
[35] Lambert-Diani, J., and Rey, C., 1999, "New Phenomenological Behavior Laws for Rubbers and Thermoplastic Elastomers," Eur. J. Mech A Solids, **18**(6), pp. 1027–1043.
[36] Amin, A., Lion, A., Sekita, S., and Okui, Y., 2006, "Nonlinear Dependence of Viscosity in Modeling the Rate-Dependent Response of Natural and High Damping Rubbers in Compression and Shear: Experimental Identification and Numerical Verification," Int. J. Plast., **22**(9), pp. 1610–1657.
[37] Lion, A., 1996, "A Constitutive Model for Carbon Black Filled Rubber: Experimental Investigations and Mathematical Representation," Contin. Mech. Thermodyn., **8**(3), pp. 153–169.
[38] Roland, C., Twigg, J., Vu, Y., and Mott, P., 2007, "High Strain Rate Mechanical Behavior of Polyurea," Polymer, **48**(2), pp. 574–578.
[39] Fu, X., Wang, Z., Ma, L., Zou, Z., Zhang, Q., and Guan, Y., 2020, "Temperature-Dependence of Rubber Hyperelasticity Based on the Eight-Chain Model," Polymers, **12**(4), p. 932.
[40] Diani, J., and Le Tallec, P., 2019, "A Fully Equilibrated Microsphere Model With Damage for Rubberlike Materials," J. Mech. Phys. Solids, **124**(4), pp. 702–713.
[41] Mayumi, K., Marcellan, A., Ducouret, G., Creton, C., and Narita, T., 2013, "Stress–Strain Relationship of Highly Stretchable Dual Cross-Link Gels: Separability of Strain and Time Effect," ACS Macro Lett., **2**(12), pp. 1065–1068.
[42] Liu, M., Guo, J., Hui, C.-Y., Creton, C., Narita, T., and Zehnder, A., 2018, "Time-Temperature Equivalence in a PVA Dual Cross-Link Self-Healing Hydrogel," J. Rheol., **62**(4), pp. 991–1000.
[43] Xiang, Y., Zhong, D., Wang, P., Yin, T., Zhou, H., Yu, H., Baliga, C., Qu, S., and Yang, W., 2019, "A Physically Based Visco-Hyperelastic Constitutive Model for Soft Materials," J. Mech. Phys. Solids, **128**, pp. 208–218.